University of Alberta

Planar Moving Flap Valve Structure for Microfluidic Control

by

Lawrence Lam

A thesis submitted to the Faculty of Graduate Studies and Research
in partial fulfillment of the requirements for the degree of

Master of Science
in
Microsystems and Nanodevices

Department of Electrical and Computer Engineering

Fall 2011
Edmonton, Alberta

Abstract

This work describes the development of a planar moving flexible valve in polydimethylsiloxane (PDMS) with integrated optics components on a microfluidic device. Applying a positive pressure to a side channel, the fluid inside deforms the flexible PDMS which then redirects the flow in a main stream to an alternate output channel. Simulations of the fluid and solid interaction in two channel configurations are performed in COMSOL® using the Arbitrary Lagrangian-Eulerian (ALE) technique. As a result, the 5 μm and 10 μm flaps were able to be deformed and redirected by a moderate flow velocity. A silicon master was produced for making PDMS chips using standard replication molding technique. Using a commercial miniature peristaltic pump, a 10 μm flap is deflected in the microfabricated biochip by the fluid flowing from the side at an average flow rate of 130 μL/min in a 60 μm x 65μm channel.

Acknowledgements

I would like to express my thanks and appreciation to my supervisor, Prof. James McMullin for his support and guidance throughput this project.

I would like to thank Scott Munro and Stephanie Bozic at Nanofab for providing the necessary trainings and directions for use of their facility, and Seyed Azmayesh-Fard, Hooman Hosseinkhannazer, Zahurul Islam and Nakeeran Ponnampalam for their help in getting access to testing equipments and fabrication tips.

Finally I would like to thank my parents for their support and encouragement in my pursuit of this degree.

Table of Contents

List of Tables

List of Figures and Illustrations

List of Symbols, Abbreviations and Nomenclature

Symbol	Definition
°C	Degree Celsius
ALE	Arbitrary Lagrangian-Eulerian
CAD	Computer aid design
CF_4	Carbon tetra-fluoride
DEP	Dielectrophoresis
DRIE	Deep reactive ion etching
FACS	Fluorescence activated cell sorting
FEM	Finite element method
hr	hour
ICPRIE	Inductance-coupled reactive-ion etching
LIF	Laser-induce fluorescence
MEMS	Micro-electro-mechanical system
min	minute
O_2	Oxygen
PMT	Photomultiplier tube
PDE	Partial differential equations
PDMS	Polydimethylsiloxane
Re	Reynolds number
RIE	Reactive ion etching
SEM	Scanning electron microscope
Si	Silicon
UV	Ultraviolet
V	volt
μm	Micrometer
μL	Microliter

CHAPTER 1: INTRODUCTION

This chapter describes the development of a new sorting mechanism in flow cytometry. Brief introductions to flow cytometry, fluorescence activated cell sorting, and lab-on-a-chip research are given. The background studies done on other types of sorting mechanisms are also discussed. Finally the thesis objectives are stated in the last section.

1.1 Flow Cytometry

Flow cytometry is a technique for analyzing biological cells suspending in fluid flow. In 1947, the development of a flow cytometry device during WWII for counting colloidal particles was published by Gucker et al. [1] in the American Chemical Society Journal. Later in 1954, Wallace Coulter announced the instrument for measuring the size and population of live blood cells in fluid flow. It is based on changing the impedance of a cell suspended in a conductive liquid while passing through an aperture of a small tube. Ten years later, Fulwyler et al. [2] describes a true flow cytometry instrument for sorting live cells. Since then, flow cytometry has been used widely by health science researchers for the purpose of cell sorting.

1.2 Fluorescence-activated Cell Sorter (FACS)

A fluorescent molecule which can be selectively tagged on to a living cell absorbs a specific wavelength of light and emit longer wavelengths of light. By exciting the fluorescently labelled cells with different wavelengths of lights,

identification and sorting of different cell types can be achieved. Applying the flow cytometry technique, fluorescently-labelled cells can be detected and sorted; hence the fluorescence-based cell sorting device (FACS) is developed. In late 1960, the first FACS system was published in paper at Stanford [3]. Without the advance micro-fabricated biochip, the first FACS is able to sort cells by using glass tubes and labware to confine the fluid flow, as well as lasers and optical filters to excite and detect the fluorescence. Today, bench-top FACS has been made possible by manufacturers for laboratories to do cell research [4].

A fluorescence-based flow cytometry system typically involves one or more laser source for exciting the fluorescent molecules carried by the cells (laser-induce fluorescence, LIF). LIF systems have the advantage of narrow beam spot size to be used with small detection volume, but the selection of available laser emission wavelengths is often limited. The lamp-based fluorescence systems, on the other hand, are less common, but have a wider selection of the excitation wavelengths by using different filters and optical slits [5, 6]. Different emissions of fluorescent spectrums from different types of fluorescent molecules can be used to identify the type of cells that carried them. Typically, a sensitive detector, such as a photomultiplier tube (PMT) is required to detect the fluorescent signals. A complete FACS system also requires a passive or active sorting mechanism to manipulate and sort cells. Although conventional FACSs have been used widely in many areas including medicine, biology and immunology, they are still costly to operate [7-9]. Wollf et al. [8] demonstrated a microfabricated FACS based on hydrodynamic switching that sorts cells at a rate of 12000 cells/s. Despite the

unknown reliability and repeatability, this high-throughput FACS device is cheaper to make and has smaller footprint compared to the conventional instruments.

1.3 Lab on a Chip (LOAC)

Recently, researchers are looking to miniaturize the flow cytometry to a smaller scale in order to reduce operational cost and to provide portability for doctors to do fast on-site diagnostic [7-11]. The development of photo-lithography for microfabrication in the 1960's gave researchers a different perspective for building things small [12]. Using Micro-electro-mechanical system (MEMS) technology and integrating the necessary parts of a flow cytometer on to a biochip, the device footprints and fabrication costs can all be reduced. The integration of optics and microfluidic device (Optofluidics) is a typical example [9, 13, 14]. Besides the integration of optics and other components in microfluidic devices, the use of polydimethylsiloxane (PDMS) and ultraviolet (UV) curing material allows rapid prototyping for lower fabrication cost, and the concept of the disposable biochips [11, 13, 15].

1.4 Background on Cell Sorting Mechanism in Microfluidics

There are many methods that can be used in manipulating cells or particles in microfluidic devices. In general, they are categorized into five classes based on the type of force applied to the cells; magnetic, optical, mechanical, electrical and

other manipulation techniques [10, 16]. Attaching the magnetic antibodies or super-paramagnetic nanoparticle to any cells of interests, one can sort out the specific cell using magnetic manipulation. Although a large magnet is often required, it is considered one of the cleanest and most efficient sorting mechanisms because of the contactless operation. Optical manipulation ("optical tweezers") on the other hand is not as efficient, but it provides a non-contact and non-invasive way of manipulation. Using a high power laser, a cell can be captured at the focal point of the electric field providing a good solution for single cell analysis [17, 18]. A similar form of manipulation is called "photoacoustic tweezers", which uses pulsed laser to create acoustic wave to capture a cell or particle [19]. Mechanical manipulation obviously is a contact method. MEMS-based devices, such as the microgrippers often have complex mechanical forms and can be difficult to fabricate [20]. Dielectrophoresis (DEP), one of most commonly seen electrical manipulations and is also invasive due to the application of the high electric field [21]. Finally, another type of rarely seen sorting mechanism, hydrodynamic sorting [22], is also similar to the sorting method used here. Hydrodynamic sorting uses controlled flow to change the state of the main flow. However, hydrodynamic sorting sometimes can have back flow problem, such that the sudden pressure change affects all in the network [7]. In this work, the flap is designed to manipulate a flow and particles by closing the opening of a channel. There are also other types of planar flap structures made and designed for microfluidic purposes. Adam et al. [23] produced an upright flap structure for the microfluidic purpose using a complicated fabrication

technique. Junhui et al. [24] designed a microfluidic pump using a flap structure which is fixed at the base using a thicker SU-8 master (150 μm).

1.5 Thesis Objectives

The main focus of this research is to develop a new sorting mechanism on biochips using low cost fabrication techniques and process steps. The concept is to put a deformable flap valve in the microchannel. The flap valve can be activated by flow from a side channel. An illustration of proposed new sorting mechanism based on the flap structure is shown in Figure 1.1. The top and bottoms are sealed by two other PDMS layers. Since most devices made in curable polymers are designed to move in vertical direction, the displacement is often limited by the thickness of the layer stack. More importantly, the vertical arrangement is difficult to integrate directly with microfluidic channels that are made via a mold replication technique. This design avoids that restriction.

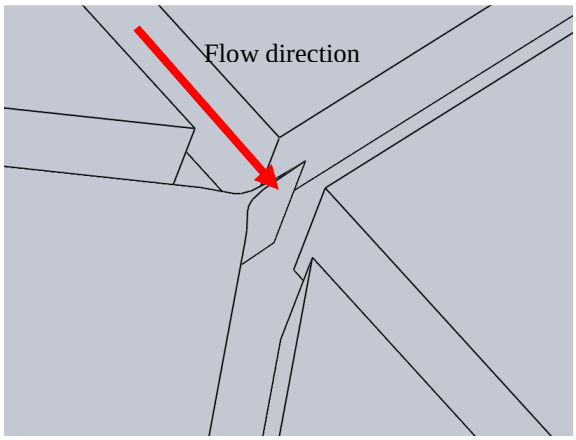

Figure 1.1: Computer aid design (CAD) drawing of the flap structure from SolidWorks®

Using a multiphysics modelling tool, COMSOL® [25], the design was optimized based on the simulation data. An estimation of the behaviour of the flap under different flow speeds can be obtained using the simulation tool, and

hence unrealistic design can be avoided. One of the advantages of using a flexible material such as PDMS in LOAC is the low Young's modulus. This means without sacrificing the device area, a low driving force is needed to deform the material to a large degree. PDMS is also much cheaper (50 times in volume-wise) than other highly used micromachining materials [26].

In order to provide future practicality to this work, many other features are also included in the design. The splitter-mixer waveguide was adopted for monitoring the flow velocity using optical signals [27]. The solid core waveguide for a simpler fabrication means was chosen [13]. All these aimed to produce highly integrated FACS devices at low cost with small footprints. The remainder sections of this thesis discuss the detail of, the simulation of flap movement in fluid flow, the fabrication processes and challenges faced in making the biochip, the testing of the flap structure using a miniature peristaltic pump, and finally the future improvement and potential application of this work.

CHAPTER 2: FLAP VALVE SIMULATION

This chapter describes the numerical methods used to simulate the deformation of the flap causing by fluid flow in the microchannel. The fluid and solid interaction problem was solved in COMSOL®, a multiphysics simulation tool based on finite element method (FEM). A parabolic velocity profile is provided to the model as the boundary condition at two inlets. The maximum flow rate of a commercially available peristaltic pump was used in the simulation to verify the feasibility of flap structures with different widths. By applying different flow velocities at the driving channel, displacements of the flap are plotted to find out the minimum driving flow velocity required for the flap to block the outlet channel. However, at maximum displacement, the simulations were interrupted due to occurrence of the inverted mesh elements. The simulation results were only meant to prove the concept of the movable flap due to fluid flow.

2.1 Introduction to Finite Element Method

The approximation made by discretization of a continuous problem is often required when an exact solution cannot be obtained using general mathematical techniques. Finite element methods are one of many numerical analyses used to solve continuous problems that are described by partial differential equations (PDE) [28]. The early form of this method was discussed by a few groups of people, such as Argyris, Turner and Courant [29]. Although Courant is considered the father of FEM for his early publication of the concept in 1942, it is Argyris

and others later supplied the details of the method [29, 30]. Since then FEM has become popular for engineering design and analysis because of its flexibility in dealing with complex geometries. FEM is found in almost all commercially available multiphysics software like ANSYS® Multiphysics, COMSOL® Multiphysics, and CFD-ACE+®. In this work, COMSOL® 3.3 was used to simulate the fluid flow and structural deformation of the flap.

2.2 Fluid and Solid Interaction

The theoretical derivation of a moving fluid acting on a flexible structure involves solving a complicated and coupled mechanical engineering problem which is not really a focus of this work. The focus of this section is to describe in detail in some workings of the COMSOL® software package, and hence to provide a reasonable prediction of the flap valve behaviour in real world. In COMSOL®, FEM procedure is used to solve the *incompressible Navier-Stokes* PDEs, and *the plane strain* PDEs for flow pressures and velocities and mechanical movement of the flexible material respectively. However, fluid and solid interaction is a nonlinear and coupled system which has free boundaries with large deformation of the solid material. This is hard to solve using a traditional grid system. The boundary conditions of the fluid and moving mesh change with time thus requiring new meshes to be generated as the simulation proceeds. In the simulation, the Arbitrary Lagrangian-Eulerian (ALE) method is applied to deal with such a problem. The following section describes the details of this method.

2.2.1 Arbitrary Lagrangian-Eulerian (ALE)

The simulation of a low viscosity fluid and the flexible flap structure was performed in COMSOL® using ALE. In short, ALE is a description of motion which can be used to solve dynamical engineering problems, in particular, the interaction of the solid and fluid. ALE is commonly used for solving problems involving the interactions between fluids and moving solids in microfluidics [31, 32]. Extracting the advantages of the two classical descriptions of kinematics, Lagrangian and Eulerian, the ALE can solve complex problems such as coupled systems with large displacement.

2.2.1.1 Lagrangian Description

The Lagrangian description of motion, named after a French mathematician, Joseph Louis Lagrange, is mainly used in solving solid structural problems. It has a characteristic of fixing the material nodes with the system grid. This allows an easier tracking of interfaces between different materials. However, because of the nature of mapping material particles to the nodes of the computational mesh grid, it cannot solve complex problem with large deformation without continuously generating new meshes due to distortions of the mesh. On the other hand, because each mesh element in Lagrangian algorithm represents the one material particle, it

has the advantage in solving history-dependent problems, such as strain hardening phenomena [33, 34].

2.2.1.2 Eulerian Description

By contrast, the Eulerian description of motion named after a Swiss mathematician, Leonhard Euler, is favoured in fluid dynamics. It is used to describe a flow or airflow at a particular instance of time. The basic idea of the Eulerian description is to focus on solving the motion of particles at a fixed point in space at a given time. In other words, the mesh elements are fixed in the Eulerian description. Figure 2.1 shows the difference between Eulerian and Lagrangian description in defining the particles' motions relative to the mesh. While the Eulerian method dominates in solving fluid flow problems, the fixed spatial grid does not allow it to solve problems with multiple interfaces (coupled system) very efficiently [33].

2.2.1.3 ALE Description

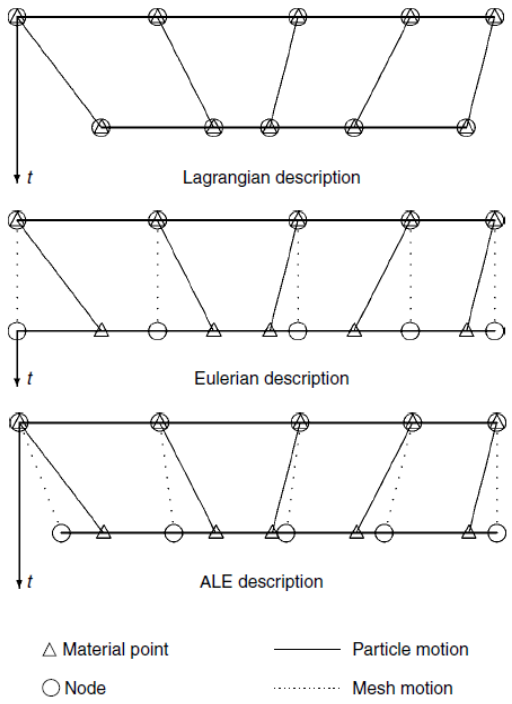

Figure 2.1: Definition of particle motion and mesh motion in the Lagrangian/Eulerian/ALE description of motion [30].

The ALE description of motion uses the advantages of both above mentioned algorithms. Fixing the material particles to a referential grid system that it inherits from the Lagrangian algorithm has the advantage of tracking interfaces between different materials. On the other hand, it also adopts the characteristics of the Eulerian description to dissociate the material particle from the spatial domain, which has the advantage of solving structural problems that have larger deformation. The characteristic of the ALE technique is to define a third domain to be the reference of the spatial formulation and the material formation, which makes this algorithm powerful and capable of solving the coupled physics problems with greater resolutions and larger flexibilities [35].

2.3 Flap Simulation

The following sections describe the modes used in the simulation model. The user's manual included in the COMSOL® package provided a basic understanding of the simulation technique applied to a simple fluid and solid interaction problem [36]. By learning the tutorials provided in the package, the simulation of the planar flap valve was accomplished and showed reasonable results.

2.3.1 Simulation Model

In COMSOL®, a two dimensional model was defined to simulate the fluid flow in microchannel. There are three basic application modes used in the ALE simulation model. The fluid mode solves the *incompressible Navier-Stokes* PDEs for the pressure and velocity of the moving fluid, the structural mechanics mode solves the *plane strain* PDEs for the deformation of flexible flap, and lastly the moving mesh mode solves the deformation of the mesh. A two dimensional model was used to reduce the computational overhead, and to avoid the gravitational force term in the Incompressible Navier-Stokes equations. The solid and fluid material properties used in the simulation can be found in Table 2.1.

Solid (PDMS-like)		**Fluid (Water-like)**	
Young's Modulus	800000 Pa	Density	1000 kg/m^3
Poisson's Ratio	0.33	Dynamic viscosity	0.001 Pa s
Thermal expansion coefficient	1.2x10^{5}1/K		
Density	965 kg/m^3		

Table 2.1: Material properties in the simulation

The mesh shape is triangular and Figure 2.2 shows the mesh density and the naming of the channel branches in the simulation model.

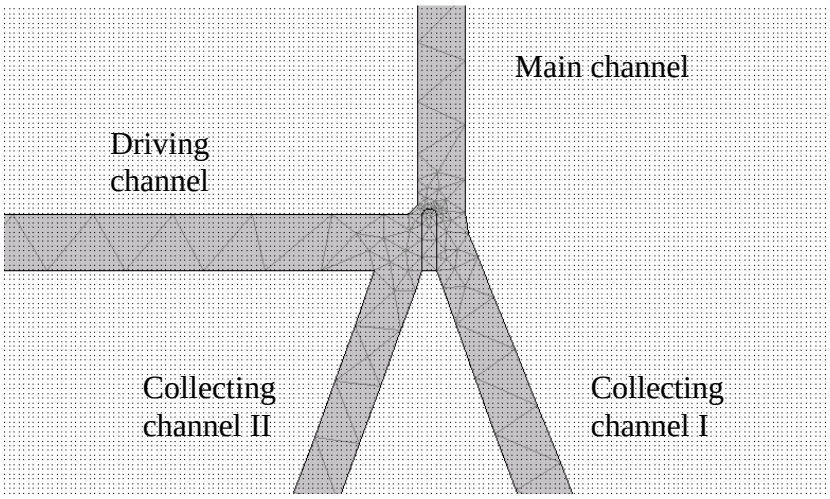

Figure 2.2: Mesh plot of the flap and microfluidic channel.

2.3.1.1 The Incompressible Navier-Stokes Application Mode

This mode is governed by the Navier Stokes equations. Assuming there is no gravitational force or any other force acting on the fluid, the body force is equal to zero. The mode also assumes that a viscous fluid with constant density is used. In other words the fluid is incompressible. The fluid properties are set to be water-like, for which the density is 1000 kg/m^3 and the dynamic viscosity is 0.001 Pa-s.

2.3.1.2 The Plain Strain Application Mode

This application mode in COMSOL® solves the deformation of the structure based on the fluid velocity. The flap which is defined as a free boundary has a Young's modulus of 800kPa and a density of 965 kg/m^3. The movement of the solid and the deformation velocity are calculated and used to define the new boundary conditions for the moving mesh and fluid equations.

2.3.1.3 The Moving Mesh Application Mode

This application mode calculates the deformation/moving of the mesh grid. Based on the deformation velocity field calculated from the plain strain mode, a new mesh is generated after each step. Three frames are defined in the model, spatial frame, mesh frame, and material frame. The spatial frame uses a fixed coordinate system, and is defined as (x,y). The material frame uses a

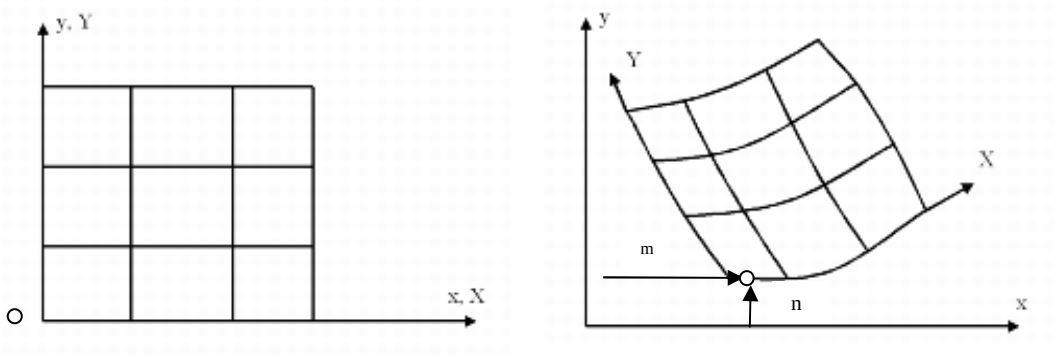

(a) **(b)**

Figure 2.3: (a) Example of an undeformed mesh, note the spatial frame (x,y) and the reference frame (X,Y) overlap. (b) Example of the distorted mesh; the reference frame (X,Y) is deformed relative to the fixed spatial frame (x,y).

reference coordinate (X,Y). The mesh frame is initially fixed to the material frame. At an instant time t, the mesh frame moves with respect to the material frame as the flap bends with increasing pressure. The deformed mesh coordinate after time t becomes (x+m,y+n,t). Figures 2.3a and 2.3b show the undeformed and deformed mesh in the fixed spatial grid.

2.3.1.4 Boundary Conditions

A water-like fluid is defined. No-slip conditions at the channel walls are applied for a viscous fluid. The condition for laminar flow was maintained during the simulation. To demonstrate this, the Reynolds number, *Re*, is calculated. *Re* is a ratio of the inertial force to viscous force, which is often used to characterize the microfluidic flow. In microfluidics, a laminar flow should have *Re* less than 100 and close to 1[9]. The equation for calculating *Re* with the density of the fluid ρ, dynamic viscosity μ, the hydraulic diameter D_h, and the centerline velocity u is,

$$Re = \frac{\rho u D_h}{\mu}$$

For a rectangular channel with width w and height h, the hydraulic diameter D_h is [37],

$$D_h = \frac{2hw}{(h+w)}$$

The density of the water-like fluid, ρ is 1000 kg/m^3, the dynamic viscosity, μ is 0.001 Pa.s and the channel width and depth is 60 μm and 65 μm for the driving

channel. The average flow velocity *u* is 0.5 m/s. Based on the above information, *Re* is 30, which is significantly less than 100, hence the flow is consider laminar .

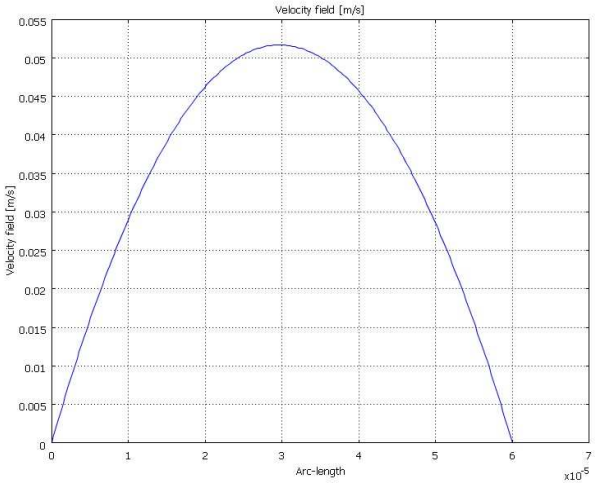

Figure 2.4: The velocity profile with a center line velocity of 0.054 m/s.

A lateral parabolic flow velocity profile is assumed at the inlet of the driving channel. The outlet is set at zero pressure. A general parabolic function is defined as shown in Figure 2.4. As fluid flows through the driving channel, the flap bends; the boundary condition at channel wall changes in the Navier-Stokes equations. The mesh is also updated according to the deformation and movement of the structure.

2.3.2 Simulation Output

Two types of configuration of the driving channel were simulated, the one-sided driving channel and the two-sided driving channel. The two-sided driving channel is designed to have two way control of flow which should help to restore the flap to its original position by pushing the flow from either side. Since the details of the work on both configurations overlap, the next section describes

the details of work done on the one-sided configuration and shows the results of the two-sided configuration.

2.3.2.1 One-sided Driving Channel Configuration

Three different widths of flap (5 μm, 10 μm, and 15 μm) were simulated at different inlet velocities in order to observe when the flap fully closes the collecting channel I. The flow velocity at the main and driving channel inlet is set to be the same. In the following section, the result of the 10 μm flap simulation is presented. Using the time-dependent solver from COMSOL®, transient analysis of the physics model is performed. Figure 2.5 shows the displacement measured

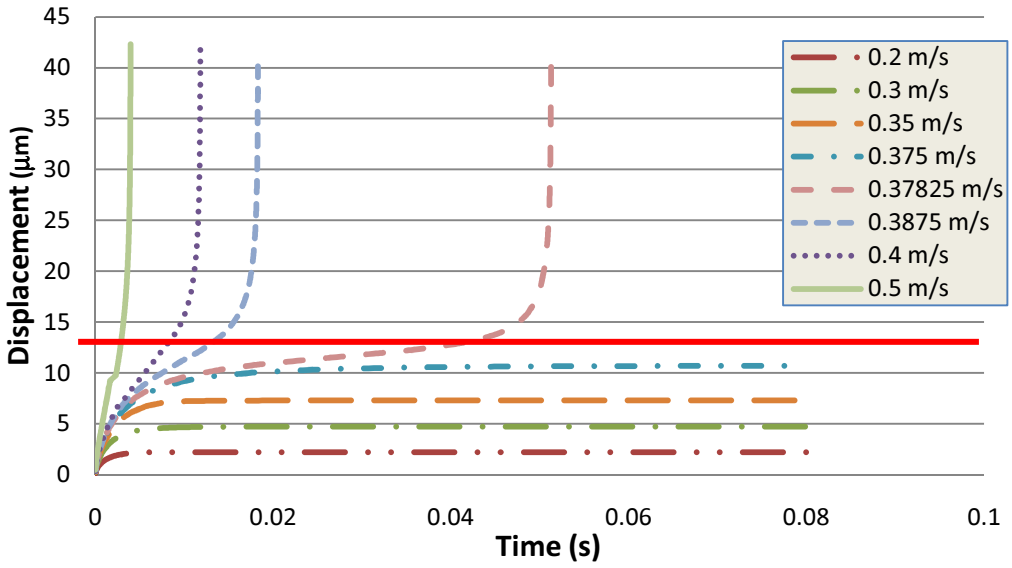

Figure 2.5: Flap displacement at different driving velocities.

from the tip of the 10 μm flap during a 0 to 0.08 s at different inlet velocities

using the transient analysis. At lower flow velocities the flap moves only slightly and reaches stable states. With faster flow speed the flap moves quickly at the beginning and then slows down until the flap moves to a position where the flow from main channel pushes the flap more effectively. Figure 2.5 shows that when displacements of the flap reach 14 μm, the flap will deform quickly and reach to maximum displacement. During the simulations of the 0.5 m/s, 0.4 m/s, 0.3875 m/s and 0.37825 m/s inlet velocities, a stable state of the flap displacement could never be reached due to the convergence errors raised from the software. However, based on the results shown in the Figure 2.5 and 2.6, we can conclude that the flap can be activated fully when the driving channel flow speed is 0.37825 m/s or more.

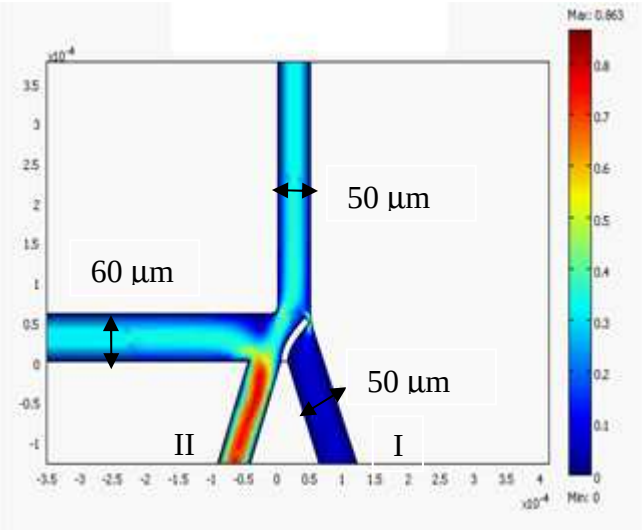

Figure 2.6: An example of two flows merging at one channel when flap deflected in a velocity profile plot.

By regenerating the mesh elements from the solution of the aborted simulation and then solving the model based on the already deformed geometric, Figure 2.6 was obtained. Figure 2.6 shows that the flap closes the *collecting channel I* almost completely. As a result, the two streams of flow from the main and driving channels merge causing a faster flow in the *collecting channel II*. The *collecting channel I* experiences nearly zero moving flow. Details

of the mesh distortion will be discussed in Section 2.3.2.3. The information about the time required for the flap to restore itself was not found from the simulation. However, quick restoration of the flexible PDMS will be demonstrated in Chapter 4 where a pulsed flow is produced by a peristaltic pump.

2.3.2.2 Two-sided Driving Channel Configuration

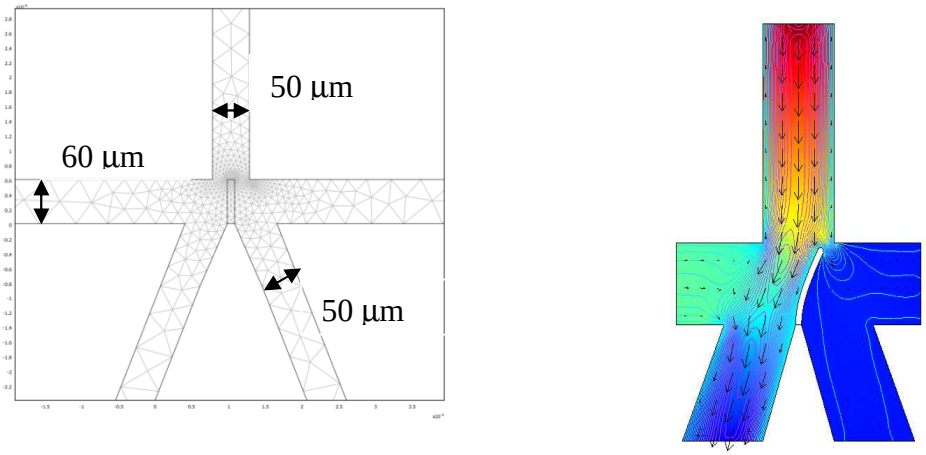

(a) **(b)**

Figure 2.7: (a) Mesh layout of the two sided configuration: (b) Simulation results showing the flap is deflected to one side.

Figure 2.7 shows the mesh element plot and the simulation results for the 10 µm flap in two-sided configuration. Figure 2.7b shows the flap being deflected to one side by the side flow coming from the right. Based on the simulation, the minimum velocity required to deflect the flap for this configuration is at least 0.5 m/s.

2.3.3 Mesh Distortion

During the simulation, computational error occurred when the deformation was too large and physical contact was made between flap and channel wall. A comparison of the undistorted and distorted meshes is shown in Figure 2.8. Figure 2.8a shows the slightly bent flap with good mesh element shape. Figure 2.8b shows when the error occurred; the triangular mesh elements become extreme and narrow as compared to other areas. This error which is called the "inverted mesh element error" in COMSOL® is common to problems, such as this one where large deformation occurs. However this problem may be solved by generating new meshes based on the deformed geometric shape using the aborted simulation condition. The simulation can be continued based on the newly optimized mesh grid, and using the latest solution to solve the model again.

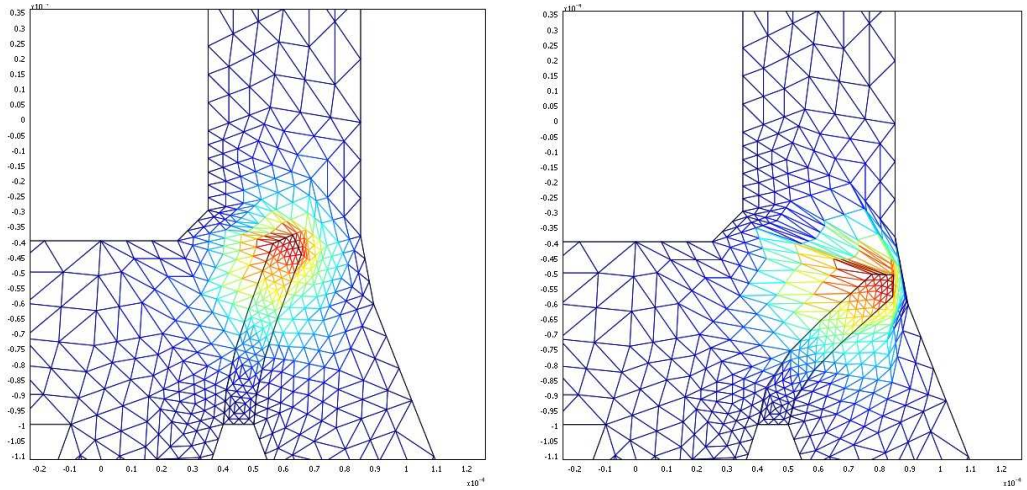

(a) **(b)**

Figure 2.8: The mesh plot of the flap with (a) small and (b) large displacement.

Nevertheless, the flap can eventually touch the wall and new physical equations must be added to the simulation model to account for the impact, friction and possibly other effects.

2.3.3.1 Summary

Simulation of the flap deflected by fluid flow in a two-dimensional physics model was demonstrated. The implementation of the ALE technique is able to generate reasonable results. In fact, based on the simulation, 0.4 m/s was found to be able to cause a 10 μm flap to deform and close the output channel. According to the product specification, a maximum flow rate of 250 μL/min is to be produced by the purchased peristaltic pump and an average flow velocity of 1.07 m/s is expected based on the designed cross-section area of the microchannel (Appendix A). Thus, it is safe to conclude that the peristaltic pump is capable of generating enough flow speed to deflect a 10 μm flap and reach maximum deformation.

CHAPTER 3: DESIGN AND FABRICATION

This chapter describes the design and fabrication method used to construct the biochips. First, the basic architecture of the microfluidic chip with integrated optical waveguides is described. The biochip is made using a standard mold replication method [11]. The BOSCH process is chosen to produce anisotropic deep silicon tranches on the mold master. The challenges of making the free standing structure using the mold replication method are discussed. A residual layer of PDMS that remains after curing causes the flap not to able to move. Additional steps for reducing excess PDMS material from the master is described which avoids the formation of the residual layer. Methods such as Doctor Blading/Screen Printing Method, PDMS dry etching, and Clamp method also described and were attempted to remove the residual layer.

3.1 Basic Architecture

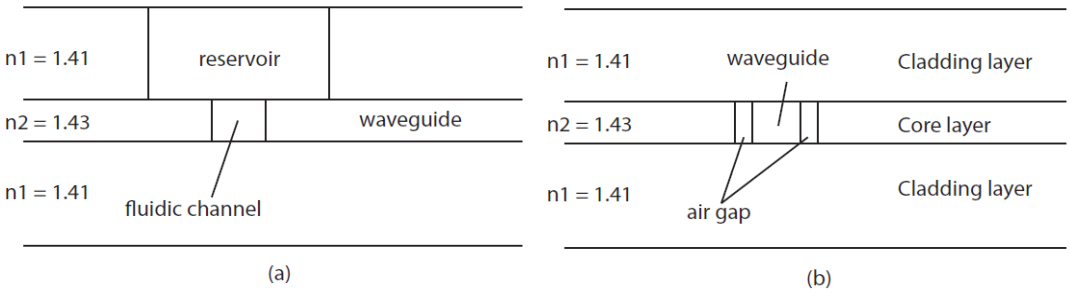

Figure 3.1: The structure of optofluidic biochips (a) End view of channel, (b) End view of waveguides showing air gap claddings.

The basic construction of the integrated biochip is shown in Figure 3.1. By sandwiching the high refractive index material between low refractive index

materials, an integrated waveguide can be produced. Fleger et al. [38] reported a method for making a PDMS biochip with integrated waveguides using a silicon mold replication technique with custom-made polysiloxanes as the core material. Azmayesh-Fard et al. [11] reported a similar fabrication method, but used two commercially available forms of PDMS elastomers.

In this design, the microfluidic channel made of high refractive index PDMS (Dow Corning 3-6121®) is sealed on the top and bottom by two PDMS layers with low refractive index (Dow Corning Sylgard 184®). Shown in Figure 3.1, the core is shielded by the claddings with low refraction index which are formed by air gaps from the sides and the regular PDMS from the top and bottom. A difficulty with this method for making free standing structure is to produce openings on both top and bottom of the thin core layer. The thickness of the core layer is limited by the etching depth of DRIE process on the Si master. A new procedure of making the thin core layers with openings is described in Section 3.2.

3.2 Fabrication Overview

The biochips were fabricated using a silicon master mold replication technique in the Nanofab. The mold replication technique is a monolithic process for making planar MEMS devices using the elastomer, PDMS. The mold master transfers the pattern to the curable PDMS prepolymer. By heating up the patterned PDMS, the features are transferred permanently as the PDMS cures. Anisotropic etching of the Si masters using the BOSCH process on the Inductively Coupled Plasma Reactive Ion Etching (ICPRIE) machine can produce straight sidewalls in

the trenches that are 60 μm wide and 65 μm deep. The liquid PDMS prepolymer is then applied manually onto the master. A clean transparency is laid upon the uncured PDMS and immediately lifted to reduce the PDMS thickness. A second transparency is then laid on the master. Two pieces of 5 inch square flat plaxiglass that sandwich the master/PDMS/transparency are clamped down using four strong metal clamps to expel excess material. The clamped mold is left in a room temperature environment for 48 hours to allow the expulsion of the PDMS. The clamped mold is then put in the oven for curing at 80 °C for 30 min. After removing the transparency, the 65 μm microfluidic layer is sealed using two thick cured PDMS wafers by O_2 plasma bonding. Due to the RIE lag effect during the DRIE process (discussed below in Section 3.2.2), the top of the PDMS flap is lower than the surrounding layer as shown in Figure 3.2, and thus does not attach to the thick PDMS layer after bonding.

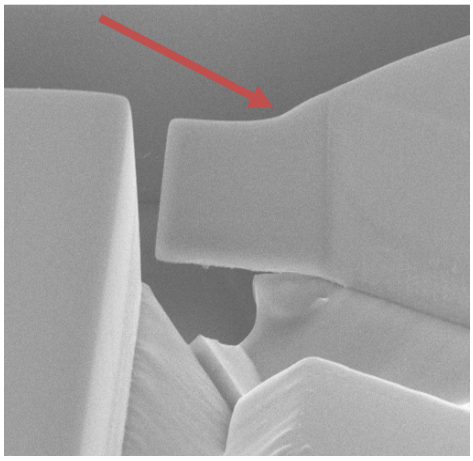

Figure 3.2: Flap finger showing the RIE lagging effect after release from Si master.

3.2.1 Deep Reactive Ion Etching (DRIE) on Silicon

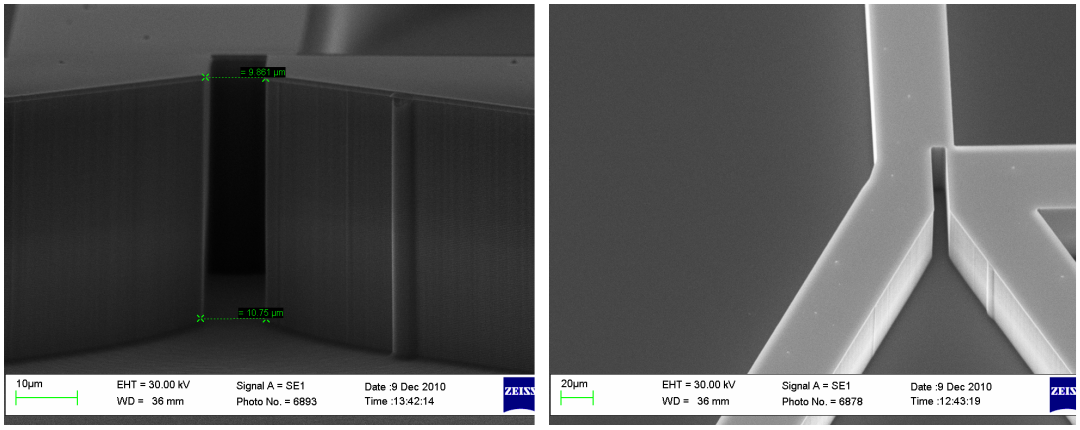

Figure 3.3: SEM of the narrow slot which will be filled with PDMS to become the movable flap (side/top view).

In this work, the BOSCH process is used to produce deep straight side walls on master for casting the microchannel and waveguides in PDMS. In the BOSCH process, etching and passivation processes are alternated. The base of the silicon trench is etched away during the etching steps and when etching stops, a passivating Teflon-like polymer that is deposited on to protect the sidewalls [39].

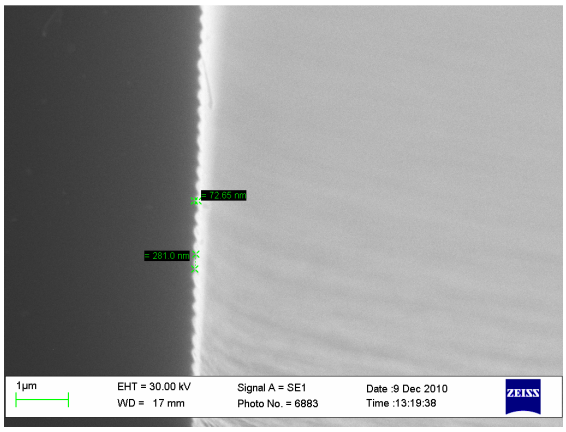

Figure 3.4: The BOSCH scallops measured for the height and depth using SEM.

In this work, after optimization, the deepest etching that can be produced without doing an extra thermo-oxidation step for increasing the oxide mask height is 65 µm. Figure 3.3 shows the results from the BOSCH

process.

The drawback of the BOSCH process is the formation of “scallops” (Figure 3.4) due to the alternating of the etching and passivation steps. The smoothness of the sidewall depends on the cycle times and the etch rate of the recipe. Higher waveguide loss can be anticipated if the sidewalls are rough. Shorter etching and passivation time steps can be used to improve the smoothness of the sidewall, but decrease the overall etch rate. There are many techniques that can be applied after the BOSCH processes to improve the smoothness of the sidewall, such as use of low concentration alkaline [40] or post-passivation in ICPRIE [41]. In this work, none of these methods were applied to improve the smoothness of the sidewalls.

3.2.2 RIE Lag

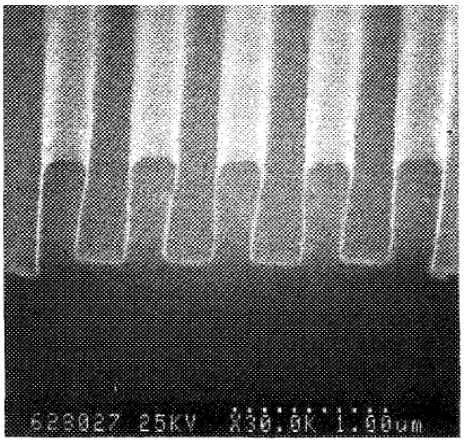

Figure 3.5: RIE lag effect - the open area etches deeper than the narrow trench [38].

During the DRIE process, the smaller feature/narrower trench etches more slowly than the wider open area, a phenomenon referred to as RIE lag [42]. Figure 3.5 shows an example of the RIE lag causing different etch depths in the open area and inside the trench. This phenomenon is typically undesirable because it causes non-uniformity on substrates after DRIE process. However, in this work this effect was a great advantage for the fabrication of the free standing flap structure. As shown in

Figure 3.6, the flap finger is much shorter than the surrounding wall. This reduces the chance of bonding to the next PDMS layer during the sealing procedure.

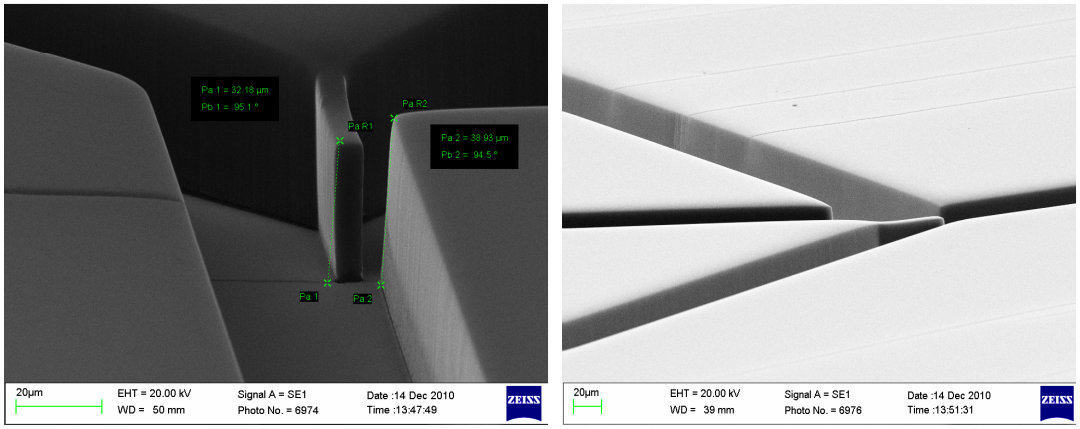

Figure 3.6: A SEM image shows that the flap figure is significant shorter than the channel wall.

3.2.3 PDMS Demolding and Bonding

The thin PDMS film is picked up by bonding to a thick PDMS. Figure 3.7 shows the 65 µm film is bonded to a thick layer. Using the RIE machine in the Nanofab, the PDMS layers are cleaned and activated by an oxygen plasma treatment and bonded together. Two pieces of PDMS were placed at the plasma chamber for 30 s of treatment, and brought into immediate contact to complete the bonding process.

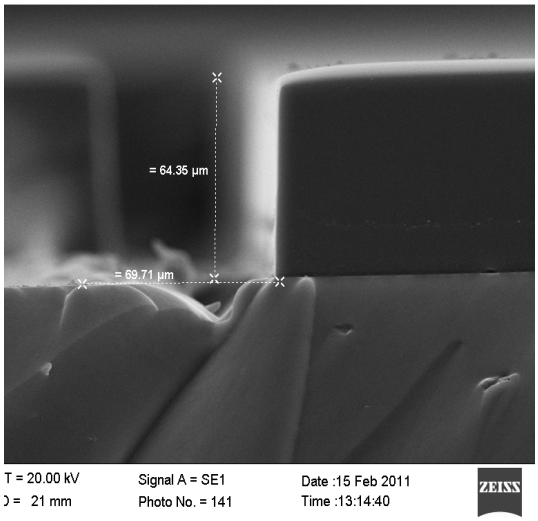

Figure 3.7: The result of demolding the 65µm PDMS film from the master.

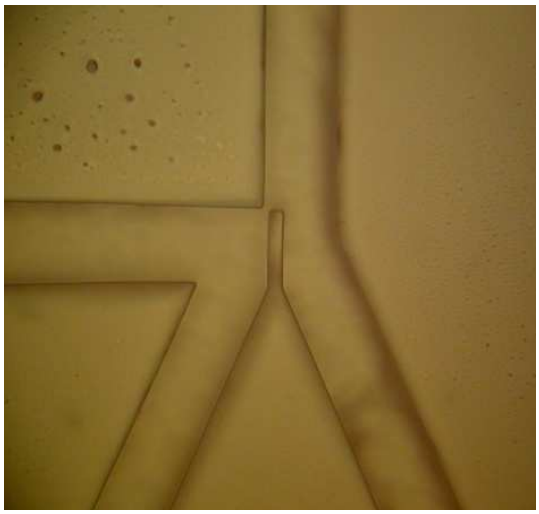

Figure 3.8: Microscope images after the microchannel and 10 μm flap sealed between two PDMS layers.

Caution must be taken when pressing the layers together; the flap can be bonded to the upper layer if pressure is applied directly on top of it. Figure 3.8 shows the final results of the sealed microchannel under the microscope.

3.2.4 Residual Layer

The residual layer shown in Figure 3.9 occurs after curing and is a known problem when using the mold replication technique [43-45]. In Figure 3.9a, the arrow shows the dark strip (residual layer) across the top of the middle layer, even in the opened area. The residual layer formed during the curing process is hard to avoid. In fact, the residual layer is virtually impossible to avoid if too much material is used. In this work, while applying the prepolymer to the master, a transparency was laid onto the material to reduce the thickness of uncured PDMS film. Although this method works occasionally, voids and air bubbles can be produced in the layer and destroy some other functions of the chip.

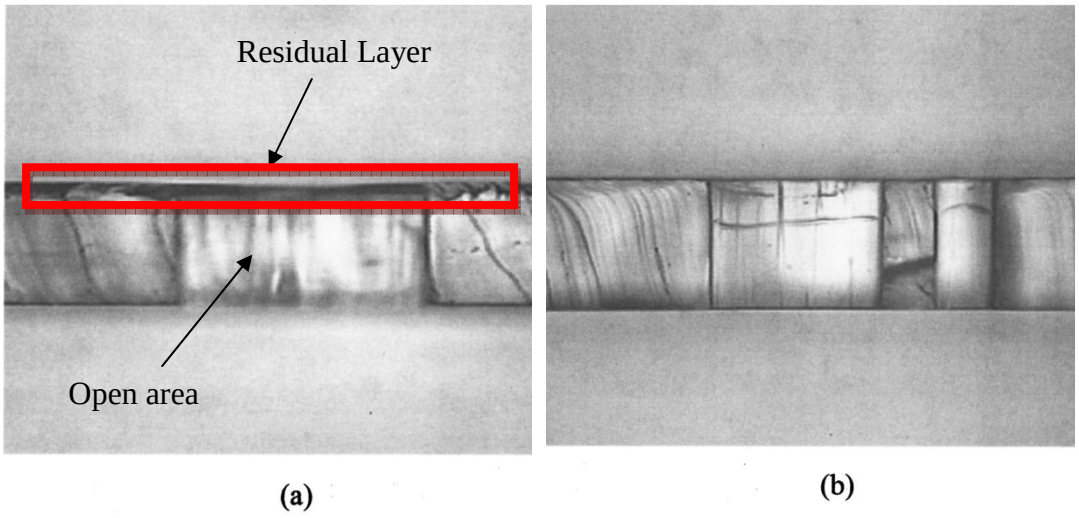

Figure 3.9: Comparison of (a) remaining residual layer and (b) lack of residual layer in PDMS biochip [39].

The challenges of making a free standing structure were faced by many other groups. The reminder of this section discusses the methods reported by other groups for dealing with this problem. The Doctor Blading method proposed by Ryu et al. [44] uses a soft blade to mechanically remove the excess material from the top of the silicon master. It was demonstrated that the about 1um of thin residual layer can still exist due to the imperfection of the Si mold surface. A post-processing by mechanical polishing is still required after the PDMS film is cured. In this work, this method was not attempted because of the need of mechanical polishing which might damage the silicon master. The sandwich molding technique or the clamp method is used in this work. Byung-Ho et al. [45] introduces this method by using clamps to squeeze out the excess material from the mold for making three-dimensional microchannel structure in PDMS. Although a stronger force can be applied using the clamp, it still produces a very

thin residual layer. By adding an additional step (discussed in Section 3.2.4.1) before this method, we found that it helped to clear the residual film on the top of the flap structure by applying the clamps directly to the top of the flap area. Figure 3.10 shows the configuration of clamps on the silicon master and the uncured PDMS.

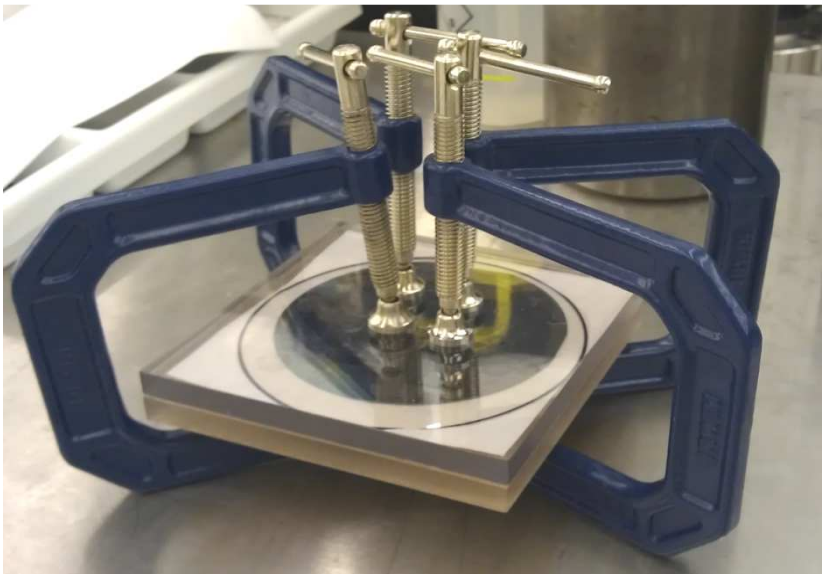

Figure 3.10: A picture of the curing process of the thin PDMS film.

There are two approaches made in this work to solve the residual layer problem. The first approach discussed in Section 3.2.4.1 tries to remove the residual film after it is formed. Since the residual layer is hard to avoid, an etching of the PDMS layer was attempted to remove it. However, because of the roughness of the surface on PDMS film after etching, this method is abandoned. The second approach discussed in Section 3.2.4.2 is a preventative method which tries to reduce the excess material during casting. This method, called the “Lift-off Method”, uses a clean transparency to lift up the excess material from the

master. By combining this method with the clamp method, a free standing structure was successfully produced. The next two sections discussed the details of the two methods attempted in this work.

3.2.4.1 PDMS Dry Etching

Garra et al. [43] reported a drying etching recipe with a etch rate of 20 μm /hr. In this work, the cured PDMS film with residual layer is left on the silicon master and etched in a reactive ion etch (RIE) chamber. Carbon tetrafluoride (CF_4) gas is used as etchant in the RIE chamber. By applying their recipe, no similar result would be found using the RIE tool in Nanofab. Although the difference in height on several wafer locations was observed, the etch rate was very low. The transparency and smoothness of PDMS layer was destroyed after the etching process. Eon et al. [46] reported that silicon-oxide-like products can be formed in the first 5 seconds of the oxygen-based etching process and resulting in a rough surface. Shown in Figure 3.11, the loss of clarity from PDMS film is actually a rough surface full of small dips. Such a rough surface prevents the bonding with the next PDMS layer even after the oxygen plasma surface treatment.

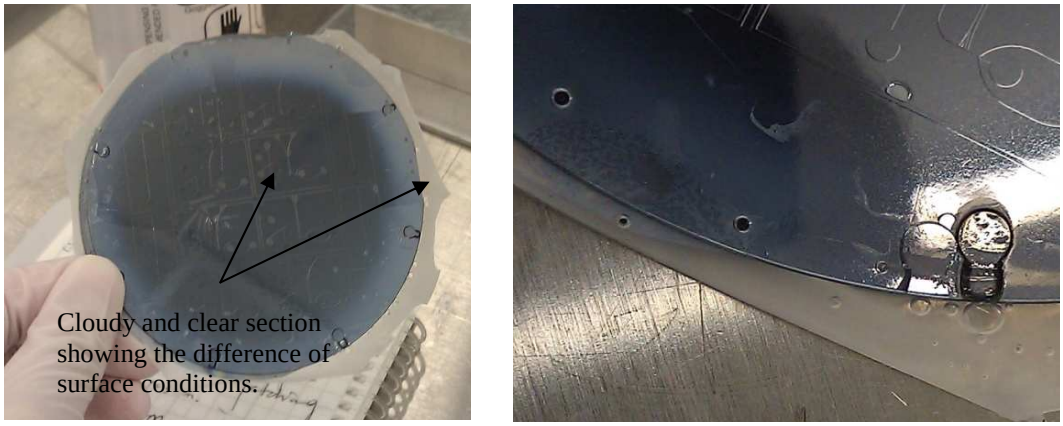

(a) **(b)**

Figure 3.11: The conditions of the PDMS film after the RIE plasma etching (a) far-view (b) close-up on PDMS film.

3.2.4.2 "Lift-off" Method

After studying and attempting the methods described above, a new method was developed. After manually applying the PDMS on to the wafer, a transparency is laid on top of the uncured PDMS material and picked up right away. This additional step is found to be efficient in lowering the height of the uncured PDMS film to the level below the silicon feature. Although it does not allow a precise control of the film thickness, the result shows that it is able to produce a planar microchannel with openings. In Figure 3.12 and 3.13, the profilmeter measurement shows that the PDMS film is lower than raised features on different location by 7 ~ 8 μm. Based on the data shown in Figure 3.12 and 3.13, it was proved that this method is good in preventing the formation of the residual layer. In fact, by applying this procedure prior to the clamping method, the planar movable flap was successfully fabricated.

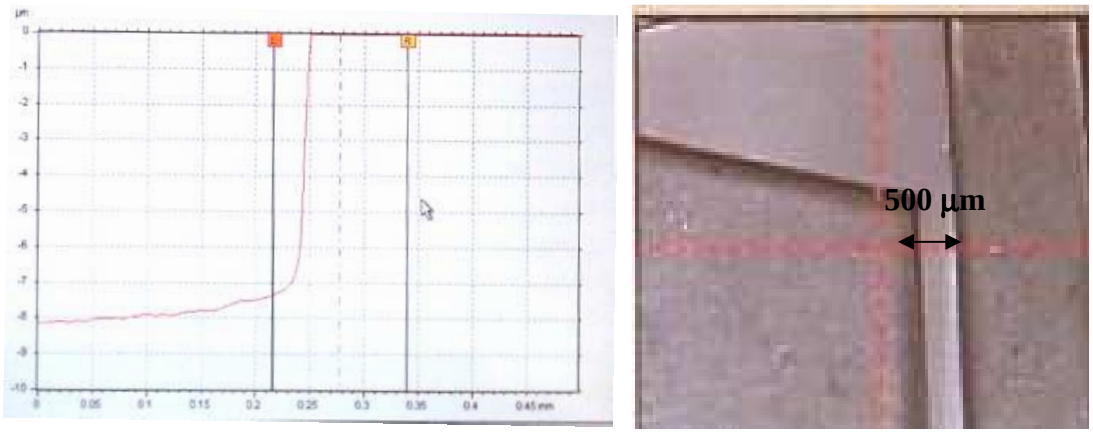

(a) **(b)**

Figure 3.12: (a) The Alpha Step results for height difference measurement over 500 μm at the location shown in the camera view in (b).

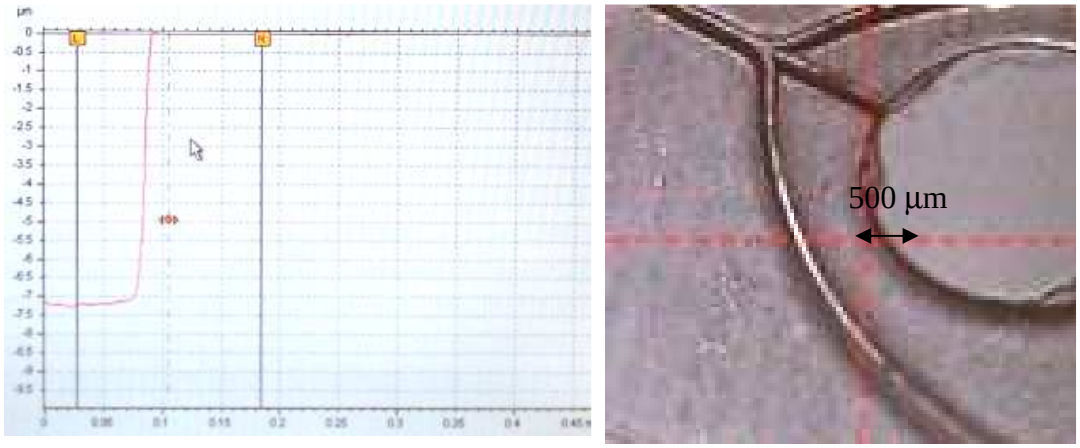

(a) **(b)**

Figure 3.13: (a) Another Alpha Step results for height difference measurement over 500 μm at the location shown in the camera view in (b).

3.3 Design Overview

The mask for lithography was drawn using L-Edit® based on the results from the COMSOL® simulation. There are three different designs of the biochips. Each design incorporates one of the two waveguide parts which will be discussed later in this chapter. Figure 3.14 shows the overview of all three designs. All

designs have the same footprint, 17 mm wide and 13.5 mm long. The 15 μm flap was not included in the mask as a much higher driving flow speed would have been required based on the simulation results.

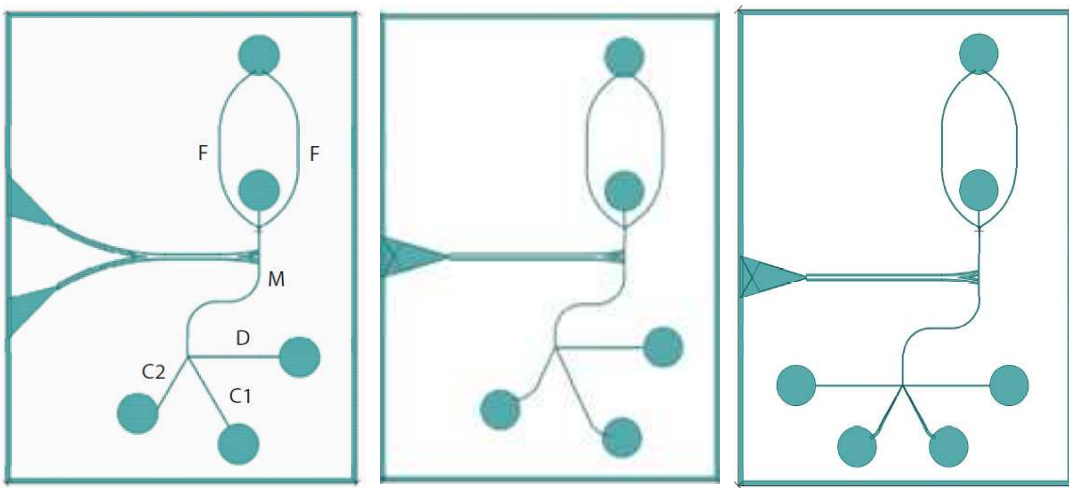

One-sided with 5um flap with channel labelling see Table 3.1 for detail description

One-sided with 10 um flap

Two-sided with 10 um flap

Figure 3.14: Overview of the design drawings.

The size of the reservoir was chosen to be 2 mm which works with plastic syringe tips for connecting plastic tubing. In the two-sided configuration, the collecting channels were designed with varying channel widths to reduce the chance of clogging of the particles. All dimensions are listed in Table 3.1. The etch depth is 65 μm throughout the master. See appendix A for details of the mask drawing.

	One sided Configuration (μm)				Two sided configuration (μm)		
	10 μm flap		5 μm flap		10 μm flap		
	Length	Width	Length	Width	Length	Width	
Collecting channel I (C1)	5052	50	3983	50	2960	50	162
Collecting channel II (C2)	3350	50	3000	50	2960	50	162
Driving channel (D)	4500	60	4500	60	4531	50	50
Main channel (M)	10314	50	10314	50	10314	50	50
Focusing channel (F)	9467	50	9467	50	9467	50	50

Table 3.1: Feature sizes for chip elements

3.3.1 Hydrodynamic Focusing

Hydrodynamic focusing is a mechanism widely used in microfluidics for focusing particles in the main flow stream [47, 48]. By squeezing the particle suspended in the fluid with side flows at uniform velocity, the particles will be focused and follow the stream line of the main flow stream. As typical microfluidic flows are laminar and have low Reynolds numbers, the particle will follow the stream line very well. It is particularly important for FACS devices to have such a stream focusing mechanism, since particles need to be identified in sequence and sorted corresponding. In this work, a two-dimensional hydrodynamic focusing mechanism is implemented as shown in Figure 3.15. It consists of two identical

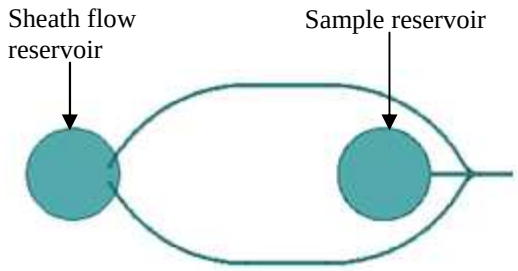

Figure 3.15: Chip configuration of the two-sided driving channel chip and its 2D hydrodynamic focusing feature.

side channels that are 50 μm wide merging at the main channel (50 μm). The two side channels will create consistent sheath flows near the two sidewalls for focusing the main stream flow.

3.3.2 Integrated Waveguides

In order to make a highly integrated flow cytometer, the integrated waveguides were incorporated in the design for fluorescence detection. [49] . A mixer and splitter waveguide was implemented to allow measuring of the velocity of the micro-beads traveling inside the microchannel. Goel and McMullin [27]

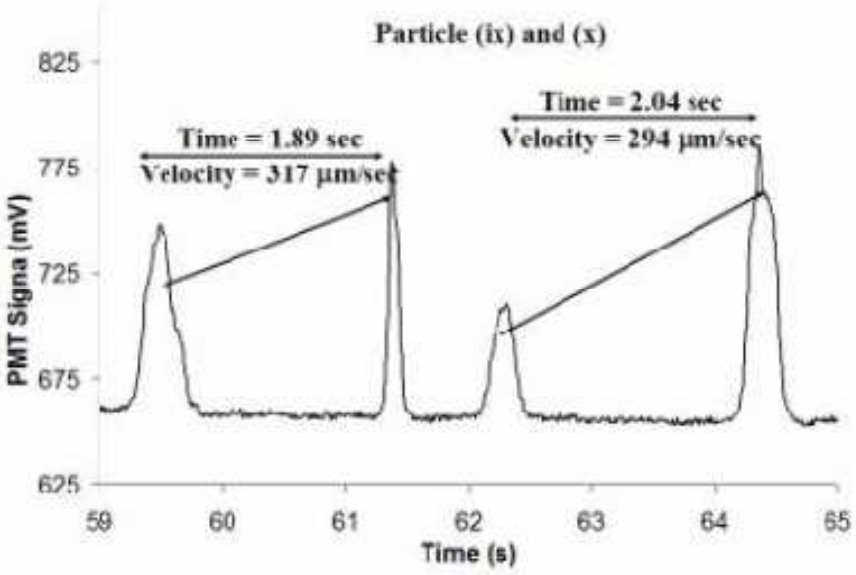

Figure 3.16: An experimental result produced by Goel and McMullin [27] **using a mixer-splitter waveguide made in SU-8.**

demonstrated this idea using SU-8 biochips in their paper for measuring the velocity of beads travelling in the flow. Depending on the type of fluorescent label that is imbedded in the polystyrene micro-beads, different wavelengths of

fluorescence can be emitted, excited by different wavelengths of laser light. The fluorescence signals coming from a particle passing the two openings of the waveguides are collected by a 1-mm plastic fibre and fed to the photo-multiplier tube (PMT). Since the distance between two openings is known, the time difference of the two fluorescence signals arriving at the PMT can be used to calculate the speed of the bead that is passing through. Figure 3.16 shows two pairs of peaks of fluorescence signals that were collected by a PMT using a large 1 mm plastic fibre. The difference in time of which the two peaks arrived to and picked up by the PMT is only depends on the speed of the beads travelling by.

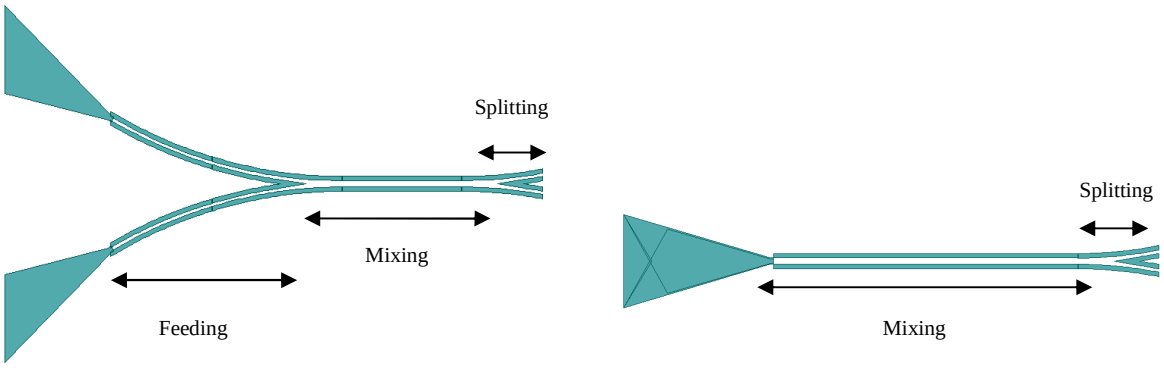

Figure 3.17: Layout of the splitter-mixer waveguides (a) and the splitter waveguide (b) from L-edit

Two different types of waveguides are included on the mask shown in Figure 3.17. The one without a feeding section is designed to work with pre-mixed light. Table 3.2 describes the dimension details of the two waveguide designs.

	Feeding (μm)		Mixing (μm)		Splitting (μm)	
	Length	Width	Length	Width	Length	Width
Mixer- splitter Waveguide	-	-	7829	140	1039	70
Splitter Waveguide	4730	70	4389	140	1039	70

Table 3.2: Details of the waveguides

3.4 Finished Biochip

(a) **(b)**

Figure 3.18: Final products (a) one-sided configuration (b) two-sided configuration.

The final product is shown in Figure 3.18. A thicker layer is used to provide stronger support when the plastic tips are inserted into the holes. The testing results presented in the following section are all based on one chip which is a one-sided configuration with 10 μm flap. Many of the chips were missing the flaps which were detached during the demolding process, or were never formed because of contamination of the Si master.

CHAPTER 4: TEST AND RESULTS

This chapter describes the details of testing the flap structure using two identical commercial miniature peristaltic pumps. The simplified drawing of the testing setup is shown below in Figure 4.1. A dc power supply is used to drive the peristaltic pumps. By switching on and off the power supply, a flow can be started and stopped. Two pieces of elastic tubing of 15 cm length are connected to the pump. The connections between the biochip and the tubing are made via plastic syringe tips.

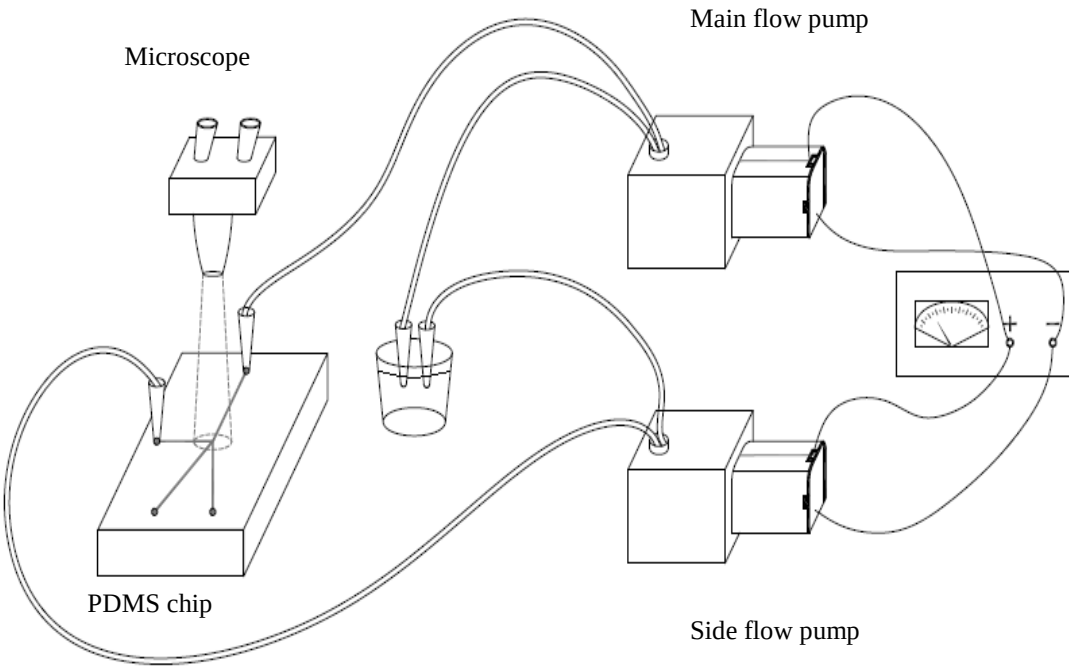

Figure 4.1: Illustration of the test setup

4.1 Miniature Peristaltic Pump

Figure 4.2: Photo of the peristaltic pump from Dolomite

Figure 4.2 shows a peristaltic pump (Dolomite [50]) operating at 0-3 V DC that was used to activate the movable flap. The peristaltic pump is driven by a miniature 3 V DC motor to produce maximum discharge pressure of 50 kPa. Similar to all peristaltic pumps, the flow is periodically pulsed (period ~2.4 s) as observed from the test data that was obtained from manufacturer shown in Figure 4.3. In the manufacturer's test results, 100cm of 250 μm I.D. elastic tubing was used to connect the flow meter and peristaltic pump. Figure 4.4 shows the average flow rate measured by the manufacturer at different supply voltages. Based on Figure 4.4 and neglecting the pressure drop in the tubing, at the normal operating voltage 1.5 V, 130 μL/min is expected to flow through the micro channel. In the (60 μm X 65 μm) channel, a maximum velocity of 0.56 m/s is expected at 1.5 V supply.

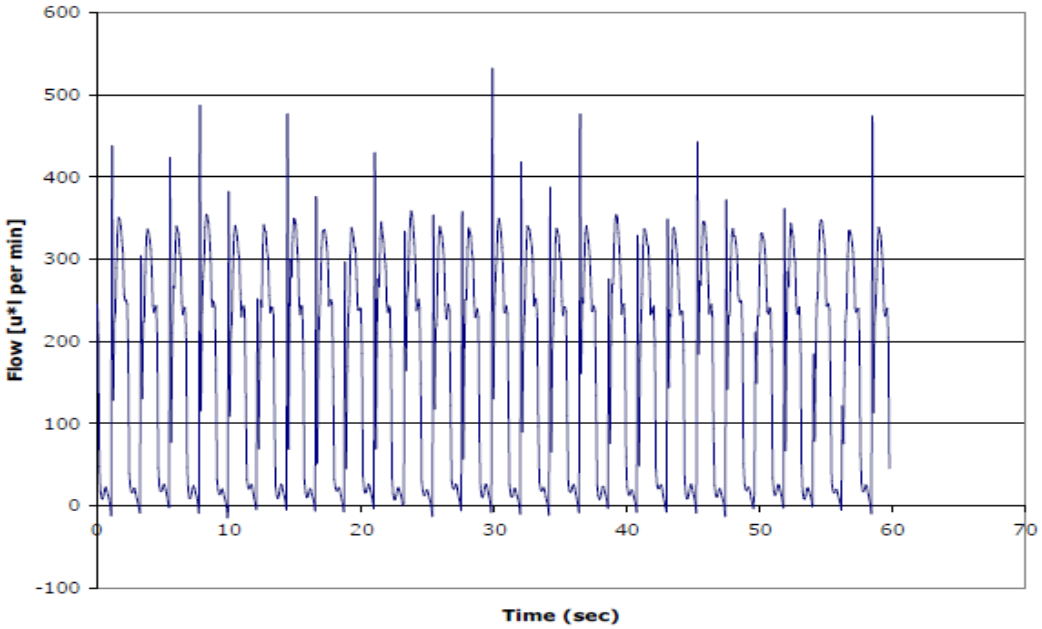

Figure 4.3: Typical Output Response for Miniature Peristaltic Pump from Dolomite at 2 V

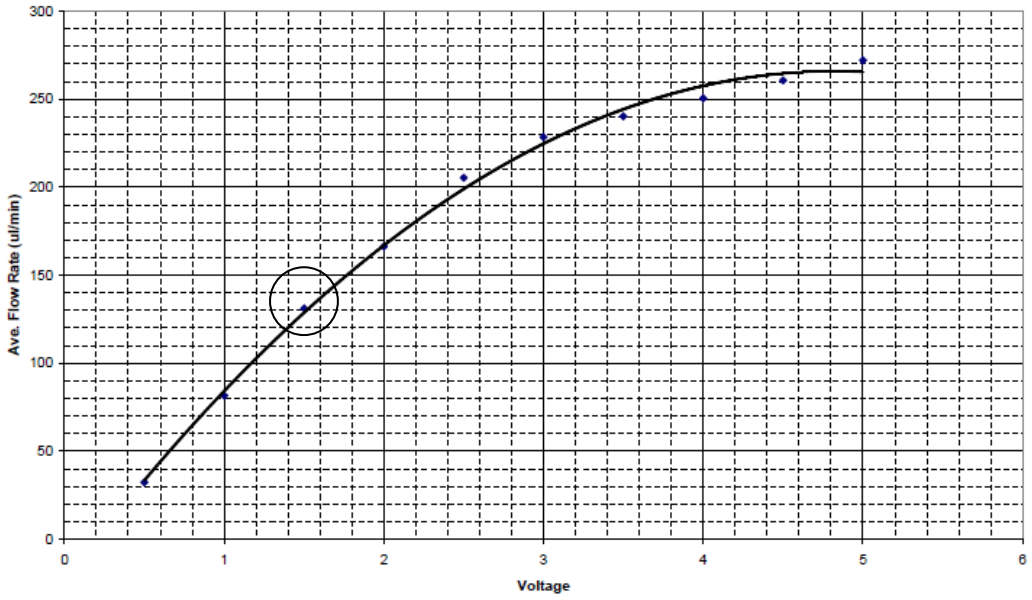

Figure 4.4: Average flow rates versus supply voltages at 2 V

4.2 Test Result

A camera was connected through the eyepiece of a stereo microscope to capture images of the flap movement. In Figure 4.5, slow oscillations of the flap which are visible to the eye are shown due to the pulsed flow characteristic from the peristaltic pump. Every 10^{th} frame from the video is shown. While the refresh rate for the camera is 30 frames per second, the result of the pictures shows that the flap oscillates with a 2.6 s period, close to the peristaltic pulsing period 2.4 s. During the low pressure point of the cycle, the flap is able to restore itself consistently.

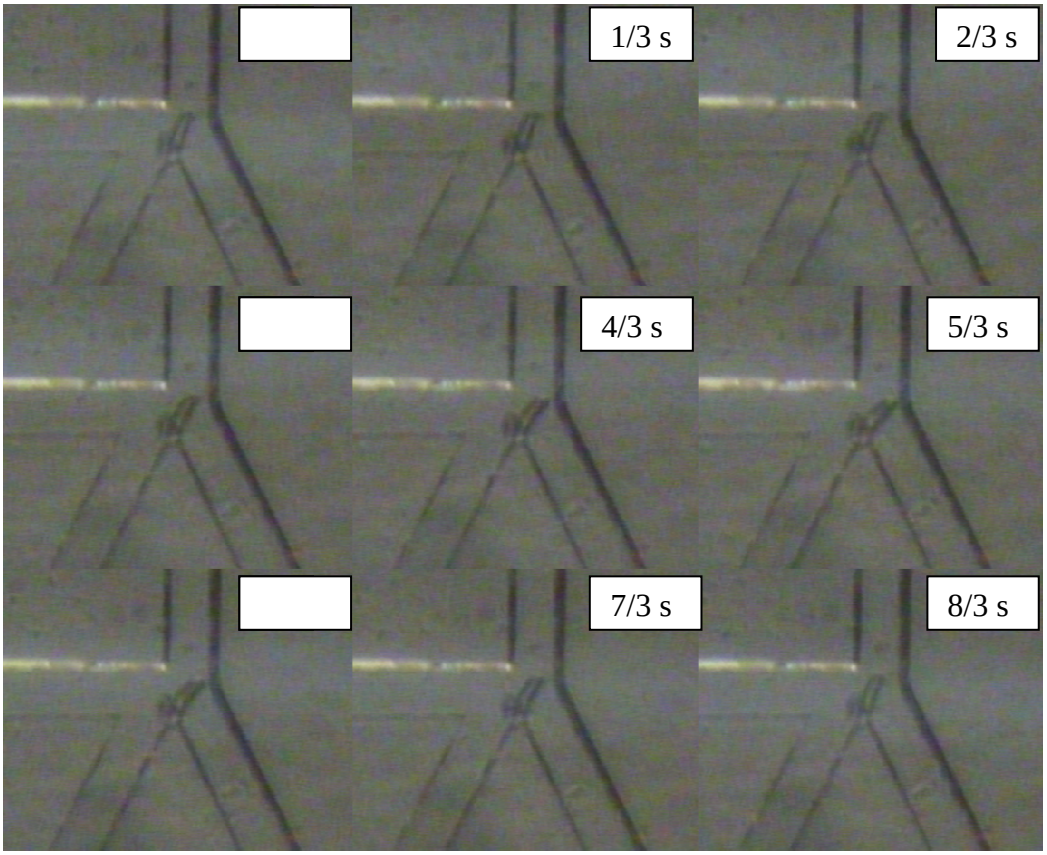

Figure 4.5: Flap movement within a cycle of the pulsed flow

Varying the supply voltages of the peristaltic pump, the maximum deflection of the flap during the oscillation of the fluid flow was recorded. Figure 4.6 shows the relationship between the maximum applied pump voltage and the maximum deflection of the flap. Note that the collecting channel I is fully closed when 1.5 V or more is applied to the pump.

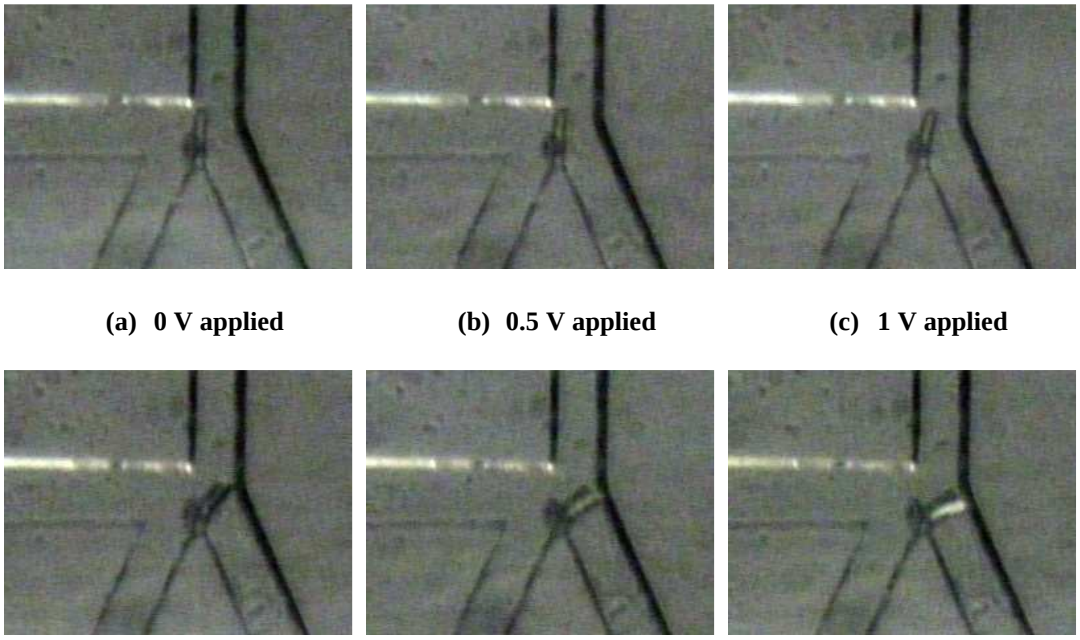

(a) 0 V applied **(b) 0.5 V applied** **(c) 1 V applied**

(d) 1.5 V applied **(e) 2 V applied** **(f) 2.5 V applied**

Figure 4.6: Flap deflection at different supply voltage

As stated, 1.5 V corresponds to an anticipated flow velocity of 0.56 m/s. Recall earlier in section 2.3.2.1 that a 10 μm flap with one-sided configuration requires 0.37825 m/s or more in order to achieve maximum deflection during the simulation. There is about 48% difference between the simulated and experimental results neglecting the backpressure of the elastic tubing used in the

experiment. The discrepancy may be due to using a two-dimensional simulation to model a three dimensional flow simulation. All in all, the movement of the planar flap structure fabricated using mold replication method has been demonstrated. The testing results show that the flap can be deflected by a pulsating flow from the driving channel and restores itself when the pressure is low.

CHAPTER 5: CONCLUSIONS

5.1 Summary of Work

This thesis describes the development a planar flap valve fabricated using a mold replication method. The large deflection of the flap was tested using a low voltage miniature peristaltic pump and the experiments showed that with less than 50 kPa inlet pressure (the maximum pressure that the peristaltic pump can provide), the flap can be deformed and can close the opening of an outlet branching channel. Such a valve may be useful for cell sorting purposes.

It was also demonstrated that the simulation data obtained from COMSOL® mutliphysics software predicts the behaviour of the flap deformation at different flow speeds. Although the fabrication process of such devices can still be improved, the overall production cost can be kept low as a result of the silicon mold replication method. Finally, this work has shown that by implementing the mold replication technique, quicker prototyping with lower cost fabrication can successfully produce a planar moving flap structure in PDMS material. Moreover, by utilizing the mutliphysics simulation tool, good understanding of the complex fluid dynamic problem can be obtained and helps to minimize design overhead. All in all, this work has shown promising results of the planar moving structure, which can be applicable to many MEMS-based devices in microfluidics. In the next section, ideas for future improvement and potential applications are described.

5.2 Suggestions for Future Work

5.2.1 Simulation

During the simulation, computation errors occur when flap is making contact to the channel wall. However, utilizing such a powerful multiphysics tool, the simulation model can be expanded by adding more equations to include effects such as friction and motion on solid interfaces. A better understanding of how the flap is restored to its original position can be obtained and making the simulation study more complete and allowing prediction of optimal performance.

5.3 Fabrication

One of the major challenges encountered during fabrication is the making of the thin functional layer and keeping the flap from contacting the top and bottom layers. The residual membrane formed on top of the silicon master is hard to avoid. The “clamping” method used in this works produces result but it is not very reliable. It works if the thickness of the PDMS is controlled, and the PDMS material must be below the features of the silicon master. However, other research groups showed promising results for removing this layer using additional process steps. Kloter et al. [51] and Mengying et al. [52] both proposed similar method of removing the residual layer by using a sacrificial layer, and these might prove useful.

5.3.1 Potential Applications

The large displacement of the flap is an advantage that may be useful in MEMS-based device since the majority of micromachined materials are crystalline or metals, which all have poor elasticity. PDMS-based devices also feature high yield points, which provide good reliability when deformed for long periods of time. An application based on the large deformation can be a microfluidic multiple species cell sorting device. With very large displacement of the flap, multiple sorting paths may be achieved with a single driving channel by carefully controlling the flow pressure.

A flexible and curable material like PDMS can be very versatile at integration with other platforms or parts. The mold replication method used on the high refractive index PDMS can produce highly integrated LOAC devices at very low cost. Integrating the deflectable flap structure with a solid core waveguide, a pressure sensor based on optical signal can be built. If light is launched into the light guiding flap, and captured with a photodetector, the amount detected will vary with the deformation of the flap at different flow pressures. A similar idea was reported by Llobera et al. [53] in a PDMS waveguides cantilever. In their work, the optical fibre is not integrated using high index PDMS. The PDMS based cantilever is used to provide mechanical support and holds the fibre. Based on the results and experience from this work, a device with similar function, very smaller footprint and better integration with the optical components can surely be achieved.

BIBLIOGRAPHY

[1] J. Gucker F.T., C. T. O'Konski, H. B. Pickard and J. Pitts J.N., "Photoelectronic counter for colloidal particles," *American Chemical Society -- Journal,* vol. 69, pp. 2422-2431, 1947.

[2] M. G. Macey, "Flow Cytometry: Principles and Applications," 2007.

[3] L. A. Herzenberg, D. Parks, B. Sahaf, O. Perez, M. Roederer and L. A. Herzenberg, "The History and Future of the Fluorescence Activated Cell Sorter and Flow Cytometry: A View from Stanford," *Clin. Chem.,* vol. 48, pp. 1819-1827, October 1, 2002.

[4] Anonymous, “Bench-top FACS.” Internet: http://www.bdbiosciences.com/ca/instruments/facsaria/index.jsp, [Aug. 23, 2011] .

[5] S. J. O. Varjo, M. Ludwig, D. Belder and M. Riekkola, "Separation of fluorescein isothiocyanate-labeled amines by microchip electrophoresis in uncoated and polyvinyl alcohol-coated glass chips using water and dimethyl sulfoxide as solvents of background electrolyte," *Electrophoresis,* vol. 25, pp. 1901-1906, 2004.

[6] Y. Mourzina, A. Steffen, D. Kalyagin, R. Carius and A. OffenhÃ¤usser, "Capillary zone electrophoresis of amino acids on a hybrid poly(dimethylsiloxane)-glass chip," *Electrophoresis,* vol. 26, pp. 1849-1860, 2005.

[7] J. Kruger, K. Singh, A. O'Neill, C. Jackson, A. Morrison and P. O'Brein, "Development of a microfluidic device for fluorescence activated cell sorting," *J Micromech Microengineering,* vol. 12, pp. 486-494, 2002.

[8] A. Wolff, I. Perch-Nielsen, U. D. Larsen, P. Friis, G. Goranovic, C. R. Poulsen, J. P. Kutter and P. Telleman, "Integrating advanced functionality in a microfabricated high-throughput fluorescent-activated cell sorter," *Lab Chip,* vol. 3, pp. 22-27, 2003.

[9] H. C. Sung, J. M. Godin, Chun-Hao Chen, W. Qiao, H. Lee and Yu-Hwa Lo, "Review Article: Recent advancements in optofluidic flow cytometer," *Biomicrofluidics,* vol. 4, pp. 043001 (23 pp.), 12, 2010.

[10] M. Toner and D. Irimia, "Blood-on-a-chip," *Annu. Rev. Biomed. Eng.,* vol. 7, pp. 77-103, 2005.

[11] S. Azmayesh-Fard, E. Flaim and J. N. McMullin, "PDMS biochips with integrated waveguides," *J Micromech Microengineering,* vol. 20, pp. 087002, 2010.

[12] M. J. Madou, Ed., *Fundamentals of Microfabrication: The Science of Miniaturization.* Boca Raton, FL.: CRC, 2002.

[13] H. Hosseinkhannazer, "Polymeric optofluidic biochips," pp. 181, 2008.

[14] S. Kim, S. Jeon, G. Yi, C. Heo, J. H. Choi and S. Yang, "Optofluidic assembly of colloidal photonic crystals with controlled sizes, shapes, and structures," *Adv Mater,* vol. 20, pp. 1649-1655, 2008.

[15] H. Hosseinkhannazer, L. Kostiuk and J. N. McMullin, "Multilayer biochips with integrated optics replicated in PMMA and PDMS," in *Photonics North 2007, June 4, 2008 - June 7,* 2008, pp. Oz Optics Ltd.; Ontario Centres of Excellence; Optoelectronics Industry Development Association; Ontario Photonics Industry Network (OPIN).

[16] C. Yi, C. Li, S. Ji and M. Yang, "Microfluidics technology for manipulation and analysis of biological cells," *Anal. Chim. Acta,* vol. 560, pp. 1-23, 2006.

[17] M. C. Wu, A. Jamshidi, S. L. Neale, M. -. Tien, A. T. Ohta and K. Yu, "Optoelectronic tweezers - A new parallel optical manipulation tool," in *TRANSDUCERS 2009 - 15th International Conference on Solid-State Sensors, Actuators and Microsystems, June 21, 2009 - June 25,* 2009, pp. 1582-1585.

[18] J. R. Moffitt, Y. R. Chemla, S. B. Smith and C. Bustamante, "Recent advances in optical tweezers," *Annual Review of Biochemistry,* vol. 77, pp. 205-228, 2008.

[19] V. P. Zharov, T. V. Malinsky and R. C. Kurten, "Photoacoustic tweezers with a pulsed laser: Theory and experiments," *J. Phys. D,* vol. 38, pp. 2662-2674, 2005.

[20] B. Solano, A. J. Gallant, G. D. Greggains, D. Wood and M. Herbert, "Low voltage microgripper for single cell manipulation," in *3rd International Conference on Smart Materials, Structures and Systems - Biomedical Applications of Smart Materials, Nanotechnology and Micro/Nano Engineering, CIMTEC 2008, June 8, 2008 - June 13,* 2008, pp. 67-72.

[21] M. Durr, J. Kentsch, T. Muller, T. Schnelle and M. Stelzle, "Microdevices for manipulation and accumulation of micro- and nanoparticles by dielectrophoresis," *Electrophoresis,* vol. 24, pp. 722-31, 02, 2003.

[22] W. Mao and A. Alexeev, "Hydrodynamic sorting of microparticles by size in ridged microchannels," *Phys. Fluids*, vol. 23, 2011.

[23] M. L. Adams, M. L. Johnston, A. Scherer and S. R. Quake, "Polydimethylsiloxane based microfluidic diode," *J Micromech Microengineering*, vol. 15, pp. 1517-1521, 2005.

[24] J. Ni, B. Li and J. Yang, "A MEMS-based PDMS micropump utilizing electromagnetic actuation and planar in-contact check valves," in *2010 International Conference on Manufacturing Engineering and Automation, ICMEA2010, December 7, 2010 - December 9*, 2010, pp. 1574-1577.

[25] Anonymous, "Multiphysics Simulation Tool." Internet: http://www.comsol.com/, [Aug. 23, 2011].

[26] S. R. Quake and A. Scherer, "From Micro- to Nanofabrication with Soft Materials," *Science*, vol. 290, pp. 1536-1540, November 24, 2000.

[27] S. Goel and J. N. McMullin, "Integrated waveguide mixer/splitter for lab-on-a-chip applications," in *Integrated Optics: Devices, Materials, and Technologies XII, January 21, 2008 - January 23*, 2008, pp. Society of Photo-Optical Instrumentation Engineers (SPIE).

[28] O. C. Zienkiewicsz, R. L. Taylor and J. Z. Zhu, *The Finite Element Method: Its Basis and Fundamentals.* Elsevier, 2005.

[29] K. K. GUPTA and J. L. MEEK, "A BRIEF HISTORY OF THE BEGINNING OF THE FINITE ELEMENT METHOD," *Int. J. Numer. Meth. Engng.*, vol. 39, pp. 3761-3774, 1996.

[30] G. Pelosi, "The finite-element method, Part I: R. L. Courant [Historical Corner]," *Antennas and Propagation Magazine, IEEE*, vol. 49, pp. 180-182, 2007.

[31] M. M. Villone, G. D'Avino, M. A. Hulsen, F. Greco and P. L. Maffettone, "Numerical simulations of particle migration in a viscoelastic fluid subjected to Poiseuille flow," *Computers and Fluids*, vol. 42, pp. 82-91, 2011.

[32] K. P. Singha and M. Kumar, "The effect of flap parameters on fluid rectification in a microfluidic diode," *Biomicrofluidics*, vol. 4, pp. 1-17, 2010.

[33] J. Huetink, P. T. Vreede and D. L. Van, "Progress in mixed Eulerian-Lagrangian finite element simulation of forming processes," *Int J Numer Methods Eng*, vol. 30, pp. 1441-1457, 1990.

[34] J. Bonet and R. D. Wood, *Nonlinear Continuum Mechanics for Finite Element Analysis.* Cambridge: Cambridge University Press, 1997.

[35] J. Donéa and A. Huerta, *Finite Element Methods for Flow Problems.* Chichester; Hoboken, NJ: Wiley, 2003.

[36] Anonymous "ALE fluid-structure interaction," COMSOL users' manual, 2008.

[37] M. Tikekar, S. G. Singh and A. Agrawal, "Measurement and modeling of pulsatile flow in microchannel," *Microfluidics and Nanofluidics,* vol. 9, pp. 1225-1240, 2010.

[38] M. Fleger and A. Neyer, "PDMS microfluidic chip with integrated waveguides for optical detection," *Microelectronic Engineering,* vol. 83, pp. 1291-1293, 2006.

[39] F. Laerme, A. Schilp, K. Funk and M. Offenberg, "Bosch deep silicon etching: Improving uniformity and etch rate for advanced MEMS applications," in *Micro Electro Mechanical Systems, 1999. MEMS '99. Twelfth IEEE International Conference on,* 1999, pp. 211-216.

[40] T. Defforge, X. Song, G. Gautier, T. Tillocher, R. Dussart, S. Kouassi and F. Tran-Van, "Scalloping removal on DRIE via using low concentrated alkaline solutions at low temperature," 2011.

[41] J. X. Gao, L. P. Yeo, M. Chan-Park, J. M. Miao, Y. H. Yan, J. B. Sun, Y. C. Lam and C. Y. Yue, "Antistick postpassivation of high-aspect ratio silicon molds fabricated by deep-reactive ion etching," *J Microelectromech Syst,* vol. 15, pp. 84-93, 2006.

[42] R. A. Gottscho, C. W. Jurgensen and D. J. Vitkavage, "Microscopic uniformity in plasma etching," *J. Vac. Sci. Technol. B,* vol. 10, pp. 2133-2147, September 1992, 1992.

[43] J. Garra, T. Long, J. Currie, T. Schneider, R. White and M. Paranjape, "Dry etching of polydimethylsiloxane for microfluidic systems," *J. Vac. Sci. Technol. A,* pp. 975-982., 2002.

[44] Kee Suk Ryu, Xuefeng Wang, K. Shaikh and Chang Liu, "A method for precision patterning of silicone elastomer and its applications," *Microelectromechanical Systems, Journal of,* vol. 13, pp. 568-575, 2004.

[45] B. -. Jo, L. M. Van Lerberghe, K. M. Motsegood and D. J. Beebe, "Three-dimensional micro-channel fabrication in polydimethylsiloxane (PDMS) elastomer," *Microelectromechanical Systems, Journal of,* vol. 9, pp. 76-81, 2000.

[46] D. Eon, L. de Poucques, M. C. Peignon, C. Cardinaud, G. Turban, A. Tserepi, G. Cordoyiannis, E. S. Valamontes, I. Raptis and E. Gogolides, "Surface modification of Si-containing polymers during etching for bilayer lithography," *Microelectronic Engineering,* vol. 61-62, pp. 901-906, 7, 2002.

[47] R. Scott, P. Sethu and C. K. Harnett, "Three-dimensional hydrodynamic focusing in a microfluidic Coulter counter," *Rev. Sci. Instrum.,* vol. 79, 2008.

[48] C. Simonnet and A. Groisman, "Two-dimensional hydrodynamic focusing in a simple microfluidic device," *Appl. Phys. Lett.,* vol. 87, pp. 1-3, 2005.

[49] C. L. Bliss, C. J. Backhouse and J. N. McMullin, "Two-colour microparticle detection in PDMS biochips with integrated optics," in *Photonics North 2007, June 4, 2008 - June 7,* 2008, pp. Oz Optics Ltd.; Ontario Centres of Excellence; Optoelectronics Industry Development Association; Ontario Photonics Industry Network (OPIN).

[50] Anonymous, "Peristaltic Pump." Internet: http://www.dolomite-microfluidics.com/webshop/pumps-peristaltic-pumps-c-38_40/mitos-miniature-peristaltic-pump-pack-of-2-p-721. [Aug. 23, 2011]

[51] U. Kloter, H. Schmid, H. Wolf, B. Michel and D. Juncker, "High-resolution patterning and transfer of thin PDMS films: Fabrication of hybrid self-sealing 3D microfluidic systems," in *17th IEEE International Conference on Micro Electro Mechanical Systems (MEMS): Maastricht MEMS 2004 Technical Digest, January 25, 2004 - January 29,* 2004, pp. 745-748.

[52] M. Zhang, J. Wu, L. Wang, K. Xiao and W. Wen, "A simple method for fabricating multi-layer PDMS structures for 3D microfluidic chips," *Lab Chip,* vol. 10, pp. 1199-1203, 2010.

[53] A. Llobera, V. J. Cadarso, K. Zinoviev, C. Dominguez, S. Buttgenbach, J. Vila and J. A. Plaza, "Poly(Dimethylsiloxane) waveguide cantilevers for optomechanical sensing," *IEEE Photonics Technology Letters,* vol. 21, pp. 79-81, 2009.

APPENDIX A

Volumetric Flow Rate to Flow Speed Conversion

Volumetric Flow Rate , **Q**

250 μL/min = (250 x 10^{-9}) / 60 m^3/min = 4.17 x 10^{-9} m^3/s

Cross-sectional Area of Microchannel, **A**

60 μm x 65 μm = 3900 μm^2 = 3900 x 10^{-12} m^2

Average Flow Speed, **V**

V = Q/A,

4.17 x 10^{-9} m^3/s / 3900 x 10^{-12} m^2 = 0.107 m/s

APPENDIX B

Description of Mask Drawing

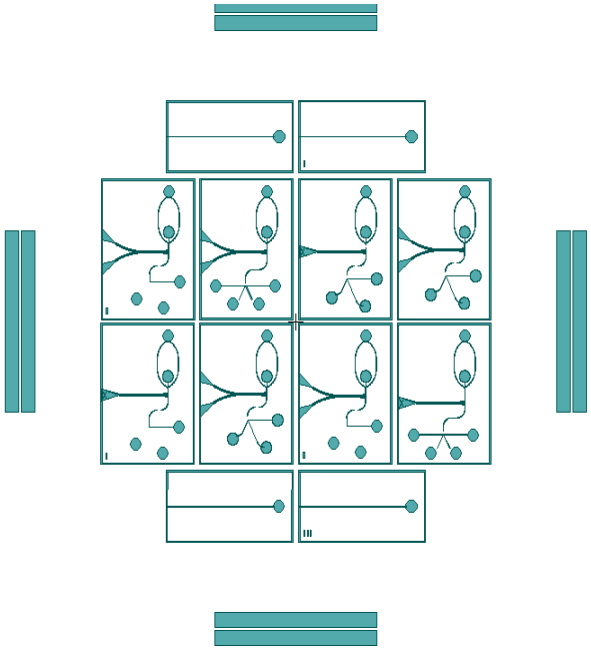

Overall mask drawing

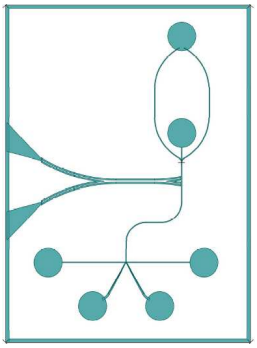

Two sided 10 µm flap design with splitter-mixer waveguide

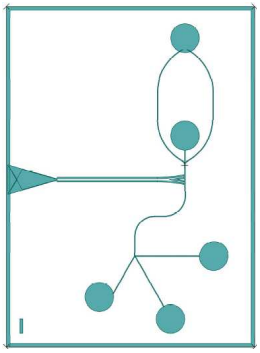

One sided 5 µm flap design with splitter waveguide

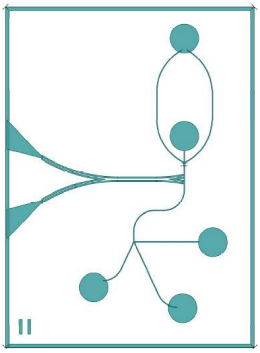

One sided 10 µm flap design with splitter-mixer waveguide

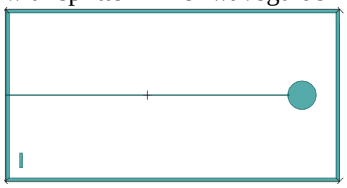

40 µm wide straight channel with reservoir

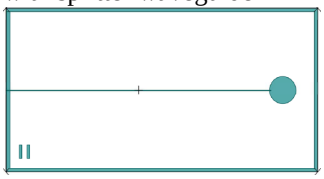

60 µm wide straight channel with reservoir

80 µm wide straight channel with reservoir